Volume 1 | Number 1 | Jan 2013 | Pages 1–100

PCCP

Physical Chemistry Chemical Physics
www.rsc.org/pccp

ROYAL SOCIETY OF CHEMISTRY

ROYAL SOCIETY OF CHEMISTRY

www.rsc.org/pccp

Competitive excited-state single or double proton transfer mechanisms for bis-2,5-(2-benzoxazolyl)-hydroquinone and its derivatives

Jinfeng Zhao†, Junsheng Chen†, Jianyong Liu*†, Mark R. Hoffmann*‡

†. *State Key Laboratory of Molecular Reaction Dynamics, Dalian Institute of Chemical Physics, Chinese Academy of Sciences, 457 Zhongshan Road, Dalian, Liaoning 116023, China.*

‡. *Department of Chemistry, University of North Dakota, Abbott Hall Room 236, 151 Cornell Street Stop 9024, Grand Forks, ND 58202-9024, USA.*

†Corresponding author. Tel: +86-411-84379195. Fax: +86-411-84675584.
†Corresponding author. E-mail: beam@dicp.ac.cn.
‡Corresponding author. E-mail: mark.hoffmann@email.und.edu.

Abstract:

The excited state intramolecular proton transfer (ESIPT) mechanisms of 2-(2-hydroxyphenyl)benzoxazole (HBO), bis-2,5-(2-benzoxazolyl)-hydroquinone (BBHQ) and 2,5-bis(5'-tert-butyl-benzooxazol-2'-yl)hydroquinone (DHBO) have been investigated using the time-dependent density functional theory (TDDFT). The calculated vertical excitation energies based on the TDDFT method reproduced the experimental absorption and emission spectra well. Three kinds of stable structures were found on the S_1 state potential energy surface (PES). A new ESIPT mechanism that differs from the one proposed previously (Mordzinski *et al*. *Chem. Phys. Lett*., 1983, **101**, 291. and Lim, *et al*. *J. Am. Chem. Soc*., 2006, **128**, 14542.) is proposed. The new mechanism includes the possibility of simultaneous double proton transfer, or successive single transfers, in addition to the accepted single proton transfer mechanism. The hydrogen bond strengthening in the excited state was based on primary bond lengths, angles, IR vibrational spectra and hydrogen bond energy. Intramolecular charge transfer based on the frontier molecular orbitals (MOs) also support the proposed mechanism of the ESIPT reaction. To further elucidate the proposed mechanism, reduced dimensionality PESs of the S_0 and S_1 states were constructed based on keeping the O-H distance fixed at a series of values. The potential barriers heights among the local minima on the S_1 surface imply competitive single and double proton transfer branches in the mechanism. Based on the new ESIPT mechanism, the observed fluorescence quenching can be satisfactorily explained.

1. Introduction

Excited-state reactions play important roles in the electronic properties of materials and biological systems, and have been the focus of many studies in physics, chemistry, and biology in recent years [1-9]. There has been particular recent interest in the intra- and inter- molecular hydrogen bonds in excited state since Han and co-workers proposed a new mechanism that elucidates changes of excited-state hydrogen bonds [10-16]. Up to now, the mechanisms in many different chemosensors have been well explained via hydrogen bond interactions, such as photoinduced electron transfer (PET), intramolecular charge transfer (ICT), excited state proton transfer (ESPT), fluorescence resonance energy transfer (FRET), and so forth [17-32]. In particular, excited-state intramolecular proton transfer (ESIPT), one of the most important elementary reactions in chemistry and biology [33-39], was first studied in pioneering work of Weller *et al.* more than 50 years ago [40, 41]. In those studies, methyl salicylate was studied to provide unique insights in the field of photochemistry [40, 41]. Since then, extensive studies on proton transfer (PT) reactions were performed both experimentally and theoretically [2-5, 42-45]. The fast and strong reorganization of the charge distribution derived from tautomerization makes these molecules very attractive for the design and use of fluorescence sensors, laser dyes and LEDs, UV filters, and molecular switches [46-57]. Such a vast range of applications has contributed in making the investigation of the unique phenomenon of ESIPT an active and dynamic subject of research.

Usually PT occurs in molecules containing both acidic and basic groups in close proximity that may rearrange in the electronic excited state via a proton transfer. The mechanism of the ESIPT normally includes the transfer of a hydroxyl (or amino) proton to an oxygen or nitrogen acceptor atom of a hydrogen bond already formed in the S_0 state. In effect, after the photo-excitation, the nuclear wave function of the molecule is projected on the excited-state potential energy surface and results in an unstable position of the proton. The driving force for the proton transfer is provided by the energy difference between the initial excited state and the relaxed excited state,

and, in turn, the relative kinetics could be determined by the slope of the surface connecting these two points. Many significant indications of the occurrence of proton transfer in the excited state can be evidenced using ordinary fluorescence spectroscopy. A nearly mirror symmetry between absorption and fluorescence spectra demonstrates that the nuclear configuration of the molecule and its surrounding medium remains close to that of the ground state over the timescale of the excited state lifetime, whereas the effect of the PT on the Frank-Condon factors leads to breaking up the mirror symmetry. The light emission originating from the proton-transferred state occurs at a longer wavelength, and hence red shift relative to the absorption spectrum. Therefore, it is possible to interpret unshifted wavelength emission as originating from the locally excited state, and to associate the red-shifted long wavelength emission with the product of proton transfer.

In recent years, more and more materials and biological systems, containing two protons, are of special interest [58-60, 74-80]. Lischka and co-workers reported an excited-state double proton transfer reaction in [2,2'-Bipyridyl]-3,-3'-diol, and concluded a sequential proton transfer mechanism [58]. Ando *et al*. studied a double proton transfer reaction in the 7-azaindole dimer system based on an ab initio potential energy surface and corresponding empirical valence bond model [59]. The double hydrogen transfer in electronically excited porphycene was investigated using a new procedure that could determine the reaction rate based on the analysis of fluorescence anisotropy [60]. The 2-(2-hydroxyphenyl)benzoxazole (HBO) and its derivatices, as organic light emitting and fluorescent probing materials, are interesting fluorophores [61-73]. On account of their intrinsic ESIPT properties, they have been applied to luminescent materials for PH and chemical sensing of cations or biologically relevant anions [61-66]. Bis-2,5-(2-benzoxazolyl)-hydroquinon (BBHQ), the D_2 symmetry of HBO, is reported that only one proton of BBHQ can be transferred in the S_1 state based on the nodal plane model proposed by Mordzinski *et al*. firstly [74]. Large spectral responses in absorption and emission have been reported by Chu *et al*., which demonstrates the potential of BBHQ in sensor applications, especially, for dual-channel detection of anions [75]. And except for its

red emission, the great fluorescence turn-on also indicates that it exhibits anionic sensing properties. In addition, they also found that BBHQ and its derivatives are largely responsible for the interesting optical properties in the polymer [75]. However, Weiß *et al*. suggested the existence of the excited-state double proton transferred state based on the observed vibronic spectra and wavepacket dynamics [76]. Recently, Wnuk et al. reported the single proton transfer mechanism based on experiments, while they do not deny the possibility of double proton transfer [77]. Whether the single proton transfer or the double proton transfer happens still remains a debated issue, which maybe not just concluded from the nodal plane model [74]. While the nodal plane model has been invoked in many previous works [78-80]. In particular, the four-level photochemical and photophysical excited state proton transfer process of 2,5-bis(5'-tert-butyl-benzooxazol-2'-yl)hydroquinone (DHBO) was explained by directly employing a single proton transfer [78]. The same conclusion of the single proton transfer was also reported by Chu *et al*. based on the titration absorption spectra and the steady state fluorescence spectra [75]. However, only the fluorescence detection range of 400-750 nm were reported, which ignored the long-wave limit in Reference 75. In addition, the ultrafast ESIPT process in aloesaponarin I chromophore has been reported by Nagaoka *et al*. using the nodal plane model, which also based on the conclusion of only one proton transfer [79]. However, whether the conclusion of only a single proton transfer is correct based on the nodal plane model warrants further attention and is the focus of the present study.

Consider that the potential energy barriers between one proton transferred structure to a double proton transferred structure (or from the structure before proton transfer to double proton transferred structure) cannot be experimentally obtained in general. Even when a single proton transfer occurs, the possibility that another proton can be transferred subsequently can not be obtained based on the nodal plane model. In addition, the Jasny spectrofluorimeter, used for measuring the absorption and emission spectra may be dated [74]. Moreover, spectroscopic techniques can only provide indirect information about photophysical properties and geometries. In order to give a detailed and unambigous ESIPT mechanism of a chromophore containing

two protons (such as the BBHQ chromophore), in the present work, a theoretical investigation has been performed to study both the S_0 and S_1 surfaces relevant to plausible transfer mechanisms. The investigations are based on DFT and TDDFT calculations for the ground and excited states, respectively. Specifically, minima on the S_0 and S_1 states were optimized, vertical excitation energies, IR vibrational spectra, hydrogen bond energies, the frontier molecular orbitals and homologous S_0 and S_1 states potential energy surfaces (PESs) were calculated. The extensive calculations were analyzed and provide the direct information of the ESIPT process.

The remainder of this paper is organized such as that the next section describes the computational details. Section 3 describes and discusses the results of the HBO calculations, then those on BBHQ which includes studies on larger regions of the PESs, and lastly DHBO is considered. A final section summarizes and gives the conclusions of this study.

2. Computational details

In this present work, all theoretical calculations presented were performed using the Gaussian 09 software suite [81]. Geometry optimizations of the S_0 state and the S_1 state were done using the DFT and TDDFT methods, respectively, with Becke's three-parameter hybrid exchange functional with the Lee–Yang–Parr gradient-corrected correlation functional (B3LYP) and the as 6-31+G(d) basis set [82-84]. In order to be consistent with the previous experiments, a heptane solvent was assumed; the solvent was represented using the integral equation formalism variant of the Polarizable Continuum Model (IEF-PCM) [85-88]. All S_0 geometries were optimized without constrains of bonds, angles and dihedral angles. Additional calculations were based on the unconstrained geometries obtained from the geometric optimization. Vibrational frequency calculations have been used to analyze the optimized structures, and specifically to confirm that these structures corresponded to the local minima on the S_0 PES (i.e., no imaginary frequencies). Calculations of the six lowest-lying vertical excitation energies have also been performed from the ground-state optimized structure, based on TDDFT and IEF-PCM methodologies.

To be consistent with ground-state calculations, equilibrium geometries on the S_1 surface were optimized without constraint and, as mentioned above, using the TDDFT method with B3LYP functional, IEF-PCM solvation model and 6-31+G(d) basis set. This protocol has been widely applied successfully for molecular systems, including weakly interacting systems [89-94]. Vibrational frequencies were calculated and analyzed for the optimized structures to confirm that these structures corresponded to the local minima on the S_1 PES. In addition to the unconstrained optimizations, constrained calculations on the S_0 and S_1 potential energy curves were performed based on fixing the O-H distance at a series of values. And the S_0 and S_1 PESs have been scanned by constrained optimizations and frequency analyses to obtain the thermodynamic corrections in the corresponding electronic state along with keeping the two O-H lengths both from 0.79 to 2.09 Å.

Fine quadrature grids of size 4 were employed. The self-consistent field (SCF) convergence thresholds for the energy in both the ground state and excited state optimization were set at 10^{-8} (default settings are 10^{-6}). Harmonic vibrational frequencies in the ground and excited state were determined by diagonalization of the Hessian. The excited-state Hessian was obtained by numerical differentiation of the analytical gradients using central differences and default displacements of 0.02 Bohr. The infrared intensities were determined from the gradients of the dipole moment [95].

3. Results and discussion

3.1 HBO

3.1.1 Geometric Structures and Hydrogen Bond Energy

In order to study the BBHQ chromophore more comprehensively, the proton transfer process in the related molecule HBO was investigated. All isomers of HBO, namely HBO-closed (HBO-C), non-hydrogen bonded HBO-open (HBO-O) and HBO-keto (HBO-K) (seen in Figure 1) have been performed using the computational protocol described above, including the heptane solvent, described by the IEFPCM model, to facilitate direct comparison with experiment [70]. The atomic coordinates

of HBO-C are provided in the ESI†. Some fundamental structural parameters involved in the hydrogen bond (e.g., primary bond lengths and angles) of HBO-C, HBO-O and HBO-K are shown in Table 1. It should be noted that the shortening of the proton donating bond length (O-H distance) in the HBO-O form compared to the HBO-C form demonstrates that the intramolecular hydrogen bond of HBO-C forms in the S_0 state. In addition, the elongation of the O-H bond from 0.997 Å (S_0) to 1.034 Å (S_1) and the shortening of the N···H bond from 1.812 Å to 1.765 Å with the concomitant enlargement of O-H···N angle from 145.1º to 147.4º indicates that the intramolecular hydrogen bond is strengthened in the S_1 state. Moreover, the hydrogen bond energies of both the S_0 and S_1 states have been calculated and provide intuitional evidence. The approach of calculating hydrogen bond energies are that the energy of HBO-C form minus the energy of HBO-O form, however, comprises the intrinsic assumption of ignoring the influence of the aforementioned rotation on overall geometry parameters of the concerned molecule other than simply cleavage of the hydrogen bond from the contiguous intramolecular hydrogen bond circuit [96]. The potential energy curves have been constructed for rotation of the hydroxyl moiety 180º from that in the HBO-C isomer to the non-hydrogen bonded HBO-O form (shown in Figure 2). The calculated results show that the hydrogen bond energy is 10.4 kcal/mol in the S_0 state and 12.7 kcal/mol in the S_1 state, which further indicates that the intramolecular hydrogen bond is strengthened. Therefore, based on the conclusion of the strengthened hydrogen bond in the S_1 state, proton transfer can be expected to occur more readily in the excited state than in the S_0 state.

3.1.2 Electronic Spectra and Potential Energy Curves

The absorption and fluorescence spectra of the HBO-C isomer have been calculated based on the S_0 geometry with the TDDFT protocol described earlier (see Figure 3(a)). The absorption maximun and emission maximun of HBO-C are located at 321.5 nm and 356.4 nm, respectively, which agrees well with the experimentally observed 280-330 nm and 360 nm [70]. In addition, another light emission maximum around 466.8 nm has been calculated, which is also in accordance with an

experimental value of 475 nm [70]. Hence, calculated vertical excitation energies based on the TDDFT method reproduced the experimental absorbance and fluorescence spectra well, which corroborates the methodology we adopted. Further analysis of the nature of the excited state conformations will inform qualitative discussion of charge distribution and charge transfer. The frontier molecular orbitals (MOs) of the HBO-C shows a predominantly $\pi\pi^*$-type transition from the highest occupied molecular orbital (HOMO) to the lowest unoccupied molecular orbital (LUMO) (see Figure 3(b)). In addition, it should be noted that the S_1 state involves the intramolecular charge transfer and the change of electron density in the hydroxyl moiety can directly influence the intramolecular hydrogen bonds [8-16, 26-32, 90-94] . The increased electron density of nitrogen atoms can enhance the intramolecular hydrogen bonds and promote proton transfer.

To elucidate the PT mechanism, potential energy curves on the S_0 and S_1 surfaces were constructed keeping the O-H bond distance fixed at values in the range from 0.99 Å to 2.39 Å in increments of 0.1 Å (see Figure 4). It can be seen clearly that the energy of the S_0 state increases along with lengthening of the O-H bond from its optimized length, producing a potential barrier of about 11.64 kcal/mol. However, it exhibits a barrier of only 1.98 kcal/mol between the geometry of the minimum on the S_1 state (i.e., after vertical transition) and the excited state equilibrium geometry. To summarize, the intramolecular proton transfer process of the HBO chemosensor is more likely to happen in the S_1 state.

3.2 BBHQ

3.2.1 Geometric Structures

The ground and excited state structures of the BBHQ chromophore were obtained based on the B3LYP functional, 6-31+G(d) basis set, and heptane described by the IEF-PCM solvation model, as described before. The atomic coordinates of BBHQ are provided in the ESI†. The local minima were verified to only have real vibrational frequencies. Three kinds of stable isomers were found (i.e. BBHQ, BBHQ-A (single proton transfer form) and BBHQ-B (double proton transfer form)), as can be seen as the top 3 in Figure 5; a fourth structure, denoted BBHQ-Open is the

non-hydrogen bonded open form, which has also been calculated using the same protocol, and, again, subsequent vibrational frequency analysis was performed to verify that the stationary point is indeed a local minimum. In order to describe bond lengths and angles more conveniently, atoms connected to the hydrogen bonds are labelled by numbers. Our calculated results shows that both O_1-H_2 and O_4-H_5 of BBHQ-Open form are 0.97 Å, however, they changed to be 0.99 Å for BBHQ form. Therefore, it can be concluded that the shortening of the proton donating bond length (O-H distance) in BBHQ-Open form compared to BBHQ form demonstrates the formation of the double intramolecular hydrogen bonds of BBHQ form in the S_0 state. In addition, calculated bond lengths (Å) and angles (º) of these stable structures for both the S_0 and S_1 states are listed in Table 2. It should be noted that the calculated lengths of O_1-H_2, H_2-N_3 ($H_2 \cdots N_3$), O_4-H_5 and H_5-N_6 ($H_5 \cdots N_6$) of BBHQ structure are 0.99, 1.82, 0.99 and 1.82 Å in the S_0 state, respectively, are changed to be 1.01, 1.72, 1.01 and 1.72 Å in the S_1 state. The variation in the lengths of the O_1-H_2 and O_4-H_5 bands as well as shortening of the $H_2 \cdots N_3$ and $H_5 \cdots N_6$ bonds indicates that these two intramolecular hydrogen bonds are strengthened in the S_1 state. And the O-H-N bond angle changes from 144.8º in the S_0 state to 148.1º of the S_1 state. Moreover, in view of the BBHQ-A form, it should be noted that $O_1 \cdots H_2$ changed from 1.89 Å (S_1) to 1.70 Å (S_0) with the concomitant enlargement of $O_4 \cdots H_5$-N from 126.8º to 134.1º, which indicates that the intramolecular hydrogen bond $O_4 \cdots H_5$-N is more stable than in the S_0 state. That is to say, after the single proton transfer process, BBHQ-A form of the S_1 state is likely to undergo radiative transition to the S_0 state forming the stable intramolecular hydrogen bond $O_4 \cdots H_5$-N. While, for the double proton transfer form BBHQ-B, only the stable structure exist in the S_1 state instantaneously and no stable structure found in the S_0 state, which can be found in the following discussion about the potential energy surfaces.

In addition, to geometric evidence, monitoring the spectral shifts of some characteristic vibrational modes involved in the hydrogen bonds is a very effective method to understand hydrogen bond strengthening or weakening [8-16, 90-94]. The vibrational spectra of BBHQ in the conjunct vibrational regions of the O-H stretching

modes are shown in Figure 6. In the S_0 state, the calculated O-H stretching vibrational frequency is located at 3375 cm^{-1}, whereas it changes to be 2970 cm^{-1} in the S_1 state. The large red-shift of 405 cm^{-1} can be ascribed to be due to the effect of the excited-state intramolecular hydrogen bonds O_1-H_2···N_3 and O_4-H_5···N_6, which corroborates the observation of hydrogen bond strengthening in the S_1 state. Furthermore, in order to compare the energies of the intramolecular hydrogen bonds (O_1-H_2···N_3 and O_4-H_5···N_6) between the S_0 state and the S_1 state, the energies of intramolecular hydrogen bonds were calculated based on the method mentioned in Reference 96. The energy of the double intramolecular hydrogen bond is found to be 19.72 kcal/mol in the S_0 state, however, upon the photo-excitation, it changes to be 24.75 kcal/mol in the S_1 state. Therefore, both the geometrical and energetic data support that the double intramolecular hydrogen bonds (O_1-H_2···N_3 and O_4-H_5···N_6) is strengthening in the S_1 state, which suggests the possibility of such a structure in the ESIPT reaction.

3.2.2 Electronic Spectra and Frontier Molecular Orbitals

The six-lowest lying vertical excitation energies of the BBHQ chromophore have been calculated from the optimized ground-state structure based on TDDFT/B3LYP/6-31+G(d) level using the IEF-PCM. The calculated electronic transition energies and the corresponding oscillator strengths (f) of the lowest-lying singlet excited states of BBHQ are listed in Table 3. The calculated first singlet transition ($S_0 \rightarrow S_1$) is at 419 nm, which is consistent with experimental result 418 nm [77]. And the second singlet transition ($S_0 \rightarrow S_2$) was calculated to be at 340 nm, which is also in agreement with experimental 340 nm [77]. The emission maximum of the first singlet transition ($S_1 \rightarrow S_0$) was calculated to be 479 nm; i.e. a Stokes shift of 60 nm is predicted. Moreover, we found the emission maximum from the single proton transferred form (BBHQ-A) to be located at 625 nm, which is in good agreement with experiment [74, 77]. Our calculated result for the emission peak from the most stable isomer (BBHQ-B) is 1020 nm, which was not reported in the previous experimental work [74, 75, 77]. The absence of the experimental peak in the near-IR may well be due to limitations of the spectroscopic equipment. However, if the

emission peak at 1020 nm really exists, the dynamics on the S_1 state may be more complex than inferred from the observed single proton transfer in previous experimental work. However, without positive identification of the existence or non-existence of the 1020 nm emission peak by a detector with suitable range, more cannot be said about the ESIPT mechanism.

In order to depict the nature of the electronically excited state, the calculated MOs of BBHQ in heptane solvent are displayed in Figure 7. Only the highest occupied molecular orbital (HOMO) and the lowest unoccupied molecular orbital (LUMO) are shown here, since a transition between just these two orbitals described essentially quantitatively (ca. 98.56%) the S_1 state with large oscillator strength of 0.9597. The π character of the HOMO as well as the π^* character for LUMO can be seen clearly, which allows description of the S_1 state as arising from a $\pi\pi^*$-type transition. Further understanding of the $S_0 \rightarrow S_1$ transition can be obtained by noting that the HOMO and LUMO are localized on different parts of the BBHQ, leading to a large dipole moment, and consistent with the large oscillator strength. The electron density of the hydroxyl moiety decreases and that of the N atom increases after transition from the HOMO to LUMO. In addition, the natural bond orbit (NBO) analyses are adopted to detailed investigation of the charge distribution over the atoms involved in intramolecular hydrogen bonds, which can be used as a reasonable evidence to explore the tendency of excited state proton transfer reaction. The one should be noted that the decrease of negative charge distribution about O atom of the –OH moiety from -0.698 in the S_0 state to -0.672 in the S_1 state together with the increase on the N atom from -0.419 to -0.432 based on the B3LYP/6-31+G(d) theoretical level. In other words, the S_1 state involves the intramolecular charge transfer and the change of electron density in the hydroxyl moiety, which can influence the double intramolecular hydrogen bonds directly. Moreover, the increased electron density on the nitrogen atoms can enhance the intermolecular hydrogen bonds and promote proton transfer.

3.2.3 Potential Energy Surfaces

In order to reveal the detailed mechanism of the ESIPT process in the BBHQ chromophore, all the S_0 state and S_1 state geometrical structures with fixed O_1-H_2 and O_4-H_5 bond lengths have been optimized at the DFT/B3LYP/6-31+G(d) level with the IEF-PEM solvation model of heptane. The constructed PESs of the S_0 and S_1 states as functions of the O_1-H_2 and O_4-H_5 bond lengths (ranging from 0.79 to 2.09 Å) are in Figure 8. Although some details of the surfaces may not be fully reproduced accurately by DFT/TDDFT, previous calculations have demonstrated that the method is sufficiently reliable to provide qualitatively (and even semi-quantitatively) accurate pathways for the proton transfer process [97-100]. The PES of the S_1 state, which is symmetrical, is shown in Figure 8(a) with minima labelled. The coordinates of these points are: a (0.99 Å, 0.99 Å), b (0.99 Å, 1.89 Å) and c (1.89 Å, 1.89 Å). The calculated results show that the potential energies of these minima are related by $E_a >$ $E_b > E_c$. That is to say, BBHQ-B is the most stable form of the S_1 state among these minima. In addition, in order to discuss the potential energies more exactly, the values of the minima (based on the B3LYP/6-31+G(d) calculation level) are given in Table S1 (ESI†). The potential barriers among these minima have also been calculated and are as follows: A 3.31 kcal/mol potential barrier separates point a from point b; 6.86 kcal/mol is needed to cross from point a to point c; and 3.56 kcal/mol separates point b from point c. These values indicate that both the single proton transfer process and the double proton transfer process are likely to happen in the S_1 state. In addition, the reverse proton transfer potential barriers among these minima also have been calculated, and result in a prediction of a 5.67 kcal/mol potential barrier for motion from point b to point a, 11.42 kcal/mol preventing passage from point c to point a and a 5.08 kcal/mol barrier between point c and point b. Except for the 11.42 kcal/mol potential barrier from point c to point a, which may be prohibitive, the other barriers are low enough that the reverse proton transfer processes are also likely to be feasible on the S_1 surface. Consequently, one should expect that the minima can almost coexist for the S_1 state, and that both the single proton transfer process and double proton transfer process are probable. Therefore, it should be concluded that the proton transfer process on the S_1 surface occurs as followed: a BBHQ molecule is excited

from the ground state to the S_1 state with a structure identified as point a. Then two cases exist: one case is that one proton is transfer from the hydroxyl O to an N atom along the hydrogen bond, thereby forming the b isomer; subsequently, either the other proton is transferred forming the c structure or not. It should be noted that this successive single proton transfer process is in agreement with the previous work based on wavepacket dynamics [76]. The second case is that a simultaneous transfer of both protons along the two hydrogen bonds could occur, thereby forming the structure denoted as c. In summary, single proton transfer (through BBHQ-A) and double proton transfer (through BBHQ-B) are competitive in the S_1 state. In turn, through the process of radiative transition, the BBHQ-A structure can emit fluorescence of 625 nm and BBHQ-B structure can emit fluorescence of 1020 nm, which induce the distinct bathochromic shift in their fluorescence emission spectra as compared with that of BBHQ structure (479 nm). As noted earlier, emission from the single proton transfer state has been observed experimentally, and that of the double proton transfer state is yet to be observed because of instrumental challenges. In addition, due to the barrierless process, after the radiative transition, the unstable **III** structure (shown in Figure 8(b)) can reverse single proton forming **II** structure or double protons forming **I** structure. Similarly, the **II** structure can also reverse single proton forming **I** structure due to the negligible barrier between **I** structure and **II** structure.

In addition, the DHBO [75, 78] (seen in Figure 9), as one of the derivatives of BBHQ, has also been investigated herein. The calculated methods are the same as previously described (The atomic coordinates shown in the ESI† and the calculated primary bond lengths and angles seen in Table S2). Our calculated vertical excitation energies again reproduce the experimental absorption and fluorescence spectra well except that the earlier experiment did not report an emission peak around 998.5 nm (corresponding to of DHBO-B) [75, 78]. For DHBO molecule, the absorption peak is calculated to be 415.4 nm, which is in consistent with experimental 415 nm [78] and 421 [75]. And the maximal emission peak around 590 nm reported in the experiment [78], and 616 nm also fits our calculated fluorescence peak 627.6 nm of DHBO-A

molecular (see Figure S1 ESI†) [75]. Moreover, the calculated electronic transition energies, the corresponding oscillator strengths (f) of the lowest-lying singlet excited states of DHBO and primary frontier molecular orbitals involved in the DHBO S_1 state are shown in Table S3 and Figure S2 (ESI†). Similar to the study of the BBHQ molecule (vide supra), the reduced dimensionality PESs of the S_0 and S_1 states of DHBO were constructed to determine the mechanisms of the ESIPT process (see Figure 10). The coordinates of the stable points are labelled a (0.99 Å, 0.99 Å), b (0.99 Å, 1.89 Å) and c (1.89 Å, 1.89 Å). And the calculated values of these minima are shown in Table S4 (ESI†). Our calculated results demonstrate that the potential energies are related by $E_c < E_b < E_a$. The c form (corresponding to the double proton transfer) is the most stable and the a form is the least. Moreover, the calculated results give a 5.04 kcal/mol potential barrier from point a to b; 6.61 kcal/mol from point a to point c; and 3.25 kcal/mol from point b to point c. As with BBHQ, single proton transfer and double proton transfer processes are competitive. The calculated potential barriers of the reverse proton transfer are 6.95 kcal/mol from point b to point a; 13.21 kcal/mol from point c to point a; and 6.14 kcal/mol from c to point b. Even though the potential barrier of 13.21 kcal/mol is not likely to be surmounted, the other two potential barriers are sufficiently low to allow reverse proton transfer process. Therefore, similar to the situation with the BBHQ chromophore, the single proton transfer and double proton transfer processes are competitive in the S_1 state.

4. Conclusion

In summary, detailed theoretical investigations have been performed to study the proton transfer processes of the BBHQ chemosensor and its tautomerization based on DFT and TDDFT calculations using the B3LYP exchange-correlation functional, the 6-31+G(d) one-electron basis set, and heptane solvent described by IEF-PCM. An analysis of the calculations demonstrates that hydrogen bond strengthening in the S_1 excited state, based on changes in bond lengths, angles, the IR vibrational spectra, and the energy of hydrogen bond, would facilitate the proton transfer process. Three local minima were found on the S_1 state surface. In order to explore the proton transfer

mechanism in detail, the reduced dimensionality PESs of the S_0 and S_1 states were constructed based on keeping the O-H distance fixed at a series of values. The forward and backward potential barriers among the minima points found on the S_1 PES showed the plausibility of both single and double proton transfer mechanisms. The single proton transfer occurs via the transfer of the hydroxyl proton to the N atom along the hydrogen bond, whereas the double proton mechanism transfers both protons along the two hydrogen bonds simultaneously or transfers the other proton after the single proton transfer. Based on the new ESIPT process, the phenomenon of fluorescence quenching could be explained reasonably.

This theoretical study complements earlier experimental work where available, and predicts an as yet experimentally unobserved fluorescence peak at 1020 nm (calculated value) from the double proton transfer minimum of BBHQ (demoted BBHQ-B) and at 998.5 nm from the corresponding minimum on the DHBO S_1 surface. Therefore, it is predicted (for both molecules) that more than one excited-state proton transfer mechanism should exist. In effect, we do not deny the validity of nodal plane model method for one of the plausible mechanisms, but caution that double proton transferred structures are ignored by this method. Maybe previous works based on the nodal plane model method on molecules that plausibly could contain double intramolecular hydrogen bonds, need to be re-examined with detailed calculations of the excited-state potential barriers. We hope that this study will encourage additional experimental work to corroborate or refute our prediction.

References

[1] D. Sicinska, D. G. Truhlar and P. Paneth, *J. Am. Chem. Soc.*, 2001, **123**, 7683.

[2] T. Kobayashi, T. Saito and H. Ohtani, *Nature.*, 2001, **414**, 531.

[3] M. Rini, B. Z. Magnes, E. Pines and E. T. J. Nibbering, *Science.*, 2003, **301**, 349.

[4] C. Tanner, C. Manca and S. Leutwyler, *Science.*, 2003, **302**. 1736.

[5] T. Schultz, E. Samoylova, W. Radloff, I. V. Hertel, A. L. Sobolewski and W. Domcke, *Science.*, 2004, **306**, 1765.

[6] T. J. Martinez, *Acc. Chem. Res.*, 2006, **39**, 119.

[7] W. M. Kwok, C. Ma and D. L. Phillips, *J. Am. Chem. Soc.*, 2008, **130**, 5131.

[8] G. J. Zhao, K. L. Han and P. J. Stang, *J. Chem. Theory Comput.*, 2009, **5**, 1955.

[9] D. M. Li, X. Q. Huang, K. L. Han and C. G. Zhan, *J. Am. Chem. Soc.*, 2011, **133**, 7416.

[10] G. J. Zhao and K. L. Han, *J. Phys. Chem. A.*, 2007, **111**, 2469.

[11] G. J. Zhao and K. L. Han, *J. Chem. Phys.*, 2007, **127**, 024306.

[12] G. J. Zhao, J. Y. Liu, L. C. Zhou and K. L. Han, *J. Phys. Chem. B.*, 2007, **111**, 8940.

[13] G. J. Zhao and K. L. Han, *Biophysical Journal.* 2008, **94**, 38.

[14] G. J. Zhao and K. L. Han, *J. Comput. Chem.*, 2008, **29**, 2010.

[15] S. Chai, G. J. Zhao, P. Song, S. Q. Yang, J. Y. Liu and K. L. Han, *Phys. Chem. Chem. Phys.*, 2009, **11**, 4385.

[16] G. J. Zhao and K. L. Han, *Acc. Chem. Res.*, 2012, **45**, 404.

[17] Z. C. Wen and Y. B. Jiang, *Tetrahedron.*, 2004, **60**, 11109.

[18] X. J. Peng, Y. K. Wu, J. L. Fan, M. Z. Tian and K. L. Han, *J. Org. Chem.*, 2005, **70**, 10524.

[19] G. Y. Li, G. J. Zhao, Y. H. Liu, K. L. Han and G. Z. He, *J. Comput. Chem.*, 2010, **31**, 1759.

[20] Q. Chu and Y. Pang, *Macromolecules.*, 2002, **35**, 7569.

[21] G. Y. Li and T. S. Chu, *Phys. Chem. Chem. Phys.*, 2011, **13**, 20766.

[22] Q. Chu and Y. Pang, *Macromolecules.*, 2003, **36**, 4614.

[23] J. Wang, Q. Chu, X. Liu, C. Wesdemiotis and Y. Pang, *J. Phys. Chem. B*., 2013, **117**, 4127.

[24] P. Song, J. X. Ding and T. S. Chu, *Spectrochim. Acta Part A.*, 2012, **97**, 746.

[25] W. Yi, A. Malkovskiy, Q. Chu, A. P. Sokolov, M. L. Colon, M. Meador and Y. Pang, *J. Phys. Chem. B*., 2008, **112**, 12263.

[26] Y. Wang, H. Yin, Y. Shi, M. X. Jin and D. J. Ding, *New J. Chem*. 2014, **38**, 4458.

[27] J. F. Zhao, P. Song, Y. L. Cui, X. M. Liu, S. W. Sun, S. Y. Hou and F. C. Ma, *Spectrochim. Acta Part A.*, 2014, **131**, 282.

[28] M. T. Sun, *J. Chem. Phys*., 2006, **124**, 054903.

[29] J. S. Chen, P. W. Zhou, G. Y. Li, T. S. Chu and G. Z. He, *J. Phys. Chem. B*., 2013, **117**, 5212.

[30] J. S. Chen, P. W. Zhou, S. Q. Yang, A. P. Fu and T. S. Chu, *Phys. Chem. Chem. Phys*., 2013, **15**, 16183.

[31] J. F. Zhao, J. S. Chen, Y. L. Cui, J. Wang, L. X. Xia, Y. M. Dai, P. Song and F. C. Ma, *Phys. Chem. Chem. Phys*., 2015, **17**, 1142.

[32] Q. Chu, D. A. Medvetz, M. J. Panzner and Y. Pang, *Dalton Trans*., 2010, **39**, 5254.

[33] P. L. Geissler, C. Dellago, D. Chandler, J. Hutter and M. Parrinello, *Science*., 2001, **291**, 2121.

[34] M. E. Tuckerman, D. Marx and M. Parrinello, *Nature*., 2002, **417**, 925.

[35] M. E. Tuckerman and D. Marx, *Phys. Rev. Letters*., 2001, **86**, 4946.

[36] D. Marx, M. Tuckerman, J. Hutter and M. Parrinello, *Nature*., 1999, **397**, 601.

[37] H. Chen, G. A. Voth and N. Agmon, *J. Phys. Chem. B*., 2010, **114**, 333.

[38] C. Lao-Ngam, P. Asawakun, S. Wannarat and K. Sagarik, *Phys. Chem. Chem. Phys*., 2011, **13**, 21646.

[39] L. Vilciauskas, M. E. Tuckerman, G. Bester, S. J. Paddison and K. D. Kreuer, *Nature Chemistry*., 2012, **4**, 461.

[40] H. Beens, K. H. Grellmann, M. Gurr and A. H. Weller, *Discuss. Faraday Soc.*, 1965, **39**, 183.

[41] A. H. Weller, *Prog. React. Kinet.*, 1961, **1**, 187.

[42] S. R. Meech, *Chem. Soc. Rev.*, 2009, **38**, 2922.

[43] P. Kukura, D. W. McCamant and R. A Mathies, *Rev. Phys. Chem.*, 2007, **58**, 461.

[44] T. Tahara, S. Takeuchi and K. Ishii, *J. Chin. Chem. Soc.*, 2006, **53**, 181.

[45] S. Hayashi, E. Taikhorshid and K. Schulten, *Biophys. J.*, 2009, **96**, 403.

[46] A. Sytnik and M. Kasha, *Proc. Natl. Acad. Sci. U.S.A.,* 1994, **91**, 8627.

[47] P. T. Chou, M. L. Martinez, W. C. Cooper, C. P. Chang, *Appl. Spectrosc.,* 1994, **48**, 604.

[48] P. T. Chou, S. L. Studer and M. L. Martinez, *Appl. Spectrosc.,* 1991, **45**, 513.

[49] F. B. Yu, P. Li, B. S. Wang and K. L. Han, *J. Am. Chem. Soc.*, 2013, **20**, 7674.

[50] F. B. Yu, P. Li, G. J. Zhao, T. S. Chu and K. L. Han, *J. Am. Chem. Soc.*, 2011, **133**, 11030.

[51] P. T. Chou, M. L. Martinez and S. L. Studer, *Appl. Spectrosc.,* 1991, **45**, 918.

[52] Memories and Switches; *Special issue of Chem*. ReV. 2000, 100.

[53] Y. Kubo, S. Maeda, S. Tokita and M. Kubo, *Nature.* 1996, **382**, 522.

[54] D. G. Ma, F. S. Liang, L. X. Wang, S. T. Lee and L. S. Hung, *Chem. Phys. Lett.*, 2002, **358**, 24.

[55] B. Feringa, *Ed. Wiley-VCH: Weinhein, Germany*, 2001.

[56] J. Keck, H. E. A. Kramer, H. Port, T. Hirsch, P. Fischer and G. Rytz, *J. Phys. Chem.,* 1996, **100**, 144468.

[57] J. Catalan, J. C. Delvalle, F. Fabero and N. A. Garcia, *Photochem. Photobiol.,* 1995, **61**, 118.

[58] F. Plasser, M. Barbatti, A. J. A. Aquino and H. Lischka. *J. Phys. Chem. A* 2009, 113, 8490.

[59] K. Ando, S. Hayashi and S. Kato, *Phys. Chem. Chem. Phys.*, 2011, **13**, 11118.

[60] M. Gil and J. Waluk, *J. Am. Chem. Soc.*, 2007, **129**, 1335.

[61] A. Ohshima, A. Momotake and T. Arai, *Tetrahedron Lett.*. 2004, **45**, 9377.

[62] M. Taki, J. L. Wolford and T. V. O'Halloran, *J. Am, Chem. Soc.*, 2004, **126**, 712.

[63] Y. Tian, C. Y. Chen, C. C. Yang, A. Cody Young, S. H. Jang, W. C. Chen and A. K. Y. Jen, *Chem. Mater.*. 2008, **20**, 1977.

[64] W. H. Chen, Y. Xing and Y. Pang, *Org. Lett.*, 2011, **13**, 1362.

[65] M. Santra, B. Roy and K. H. Ahn, *Org. Lett.*, 2011, **13**, 3422.

[66] J. Massue, D. Frath, G. Ulrich, P. Retailleau and R. Ziessel, *Org. Lett.*, 2012, **14**, 230.

[67] J. Massue, P. Retailleau, G. Ulrich and R. Ziessel, *New. J. Chem.*, 2013, **37**, 1224.

[68] K. Osama, Z. Abou, *Phys. Chem. Chem. Phys.*, 2012, **14**, 2832.

[69] V. S. Padalkar, P. Ramasami and N. Sekar, *Journal of Luminescence.*,2014, **146**, 527.

[70] R. Daengngern and N. Kungwan, *Chem. Phys. Lett.*, 2014, **609**, 147.

[71] J. Massue, D. Frath, P. Retailleau, G. Ulrich and R. Ziessel, *Chem. Eur. J.*, 2013, **19**, 5375.

[72] H. Roohi, F. Hejazi, N. Mohtamedifar and M. Jahantab, *Spectrochim. Acta Part A.*, 2014, **118**, 228.

[73] J. Massue, G. Ulrich and R. Ziessel, *Eur. J. Org. Chem.*, 2013, 5701.

[74] A. Mordzinski, A. Grabowska, W. Kuhnle and A. Krowczynski, *Chem. Phys. Lett.*, 1983, **101**, 291.

[75] Q. Chu, D. A. Medvetz and Y. Pang, *Chem. Mater.*, 2007, **19**, 6421.

[76] J. Weiß, V. May, N. P. Ernsting, V. Farztdinov and A. Mühlpfordt, *Chem. Phys. Lett.*, 2001, **346**, 503.

[77] P. Wnuk, G. Burdzinski, M. Sliwa, M. Kijak, A. Grabowska, J. Sepiot and J. Kubicki, *Phys. Chem. Chem. Phys.*, 2014, **16**, 2542.

[78] S. J. Lim, J. Seo and S. Y. Park, *J. Am. Chem. Soc.*, 2006, **128**, 14542.

[79] S. Nagaoka, H. Uno and D. Huppert, *J. Phys. Chem. B.*, 2013, **117**, 4347.

[80] J. Wang, Q. Chu, X. Liu, C. Wesdemiotis and Y. Pang, *J. Phys. Chem. B.*, 2013, **117**, 4127.

[81] M. J. Frisch, G. W. Trucks, H. B. Schlegel, G. E. Scuseria, M. A. Robb, J. R. Cheeseman, G. Scalmani, V. Barone, B. Mennucci, G. A. Petersson, H. Nakatsuji, M. Caricato, X. Li, H. P. Hratchian, A. F. Izmaylov, J. Bloino, G. Zheng, J. L. Sonnenberg, M. Hada, M. Ehara, K. Toyota, R. Fukuda, J. Hasegawa, M. Ishida, T. Nakajima, Y. Honda, O. Kitao, H. Nakai, T. Vreven, J. A. Montgomery Jr, J. E. Peralta, F. Ogliaro, M. Bearpark, J. J. Heyd, E. Brothers, K. N. Kudin, V. N.

Staroverov, T. Keith, R. Kobayashi, J. Normand, K. Raghavachari, A. Rendell, J. C. Burant, S. S. Iyengar, J. Tomasi, M. Cossi, N. Rega, J. M. Millam, M. Klene, J. E. Knox, J. B. Cross, V. Bakken, C. Adamo, J. Jaramillo, R. Gomperts, R. E. Stratmann, O. Yazyev, A. J. Austin, R. Cammi, C. Pomelli, J. W. Ochterski, R. L. Martin, K. Morokuma, V. G. Zakrzewski, G. A. Voth, P. Salvador, J. J. Dannenberg, S. Dapprich, A. D. Daniels, O. Farkas, J. B. Foresman, J. V. Ortiz, J. Cioslowski and D. J. Fox, Gaussian, Inc., Wallingford, CT, 2010.

[82] A. D. Becke,*J. Chem. Phys.*, 1993, **98**, 5648.

[83] C. T. Lee, W. T. Yang and R. G. Parr, *Phys. Rev. B: Condens.Matter Mater.Phys.*, 1988, **37**, 785.

[84] B. Miehlich, A. Savin, H. Stoll and H. Preuss, *Chem. Phys. Lett.*, 1989, **157**, 200.

[85] B. Mennucci, E. Cances and J. Tomasi, *J. Phys. Chem. B.*, 1997, **101**,10506.

[86] E. Cances, B. Mennucci and J. Tomasi, *J. Chem. Phys.*, 1997, **107**, 3032.

[87] R. Cammi and J. Tomasi, *J. Comput. Chem.*, 1995, **16**, 1449.

[88] S. Miertus, E. Scrocco and J. Tomasi, *J. Chem. Phys.*, 1981, **55**,117.

[89] G. J. Zhao and K. L. Han, *ChemPhysChem.*, 2008, **9**, 1842.

[90] G. Y. Liu, Y. H. Li, H. Zhang and G. H. Cui, *Commun. Comput. Chem.*, 2013, **1**, 88.

[91] M. Z. Zhang, B. P. Ren, Y. Wang and C. X. Zhao, *Commun. Comput. Chem.*, 2013, **1**, 216.

[92] D. D. Wang and G. J. Zhao, *Commun. Comput. Chem.*, 2013, **1**, 181.

[93] G. J. Zhao and K. L. Han, *J. Phys. Chem. A.*, 2007, **111**, 9218.

[94] Y. Liu and S. C. Lan, *Commun. Comput. Chem.*, 2013, **1**, 235.

[95] F. Furche and R. Ahlrichs, *J. Chem. Phys.*, 2002, **117**, 7433.

[96] P. Schuster, The Hydrogen Bond, vol. 1, North Holland, Amsterdam, The Nethelands, 1976.

[97] L. Serrano-Andres and M. Merchan, *J. Photochem. Photobiol. C. Photochem. Rev.*, 2009, **10**, 21.

[98] Y. Saga, Y. Shibata and H. Tamiaki, *J. Photochem. Photobiol. C. Photochem. Rev.*, 2010, 11, 15.

[99] P. Song and F. C. Ma, *Int. Rev. Phys. Chem.*, 2013, **32**, 589.

[100] A. L. Sobolewski and W. Domcke, *Phys. Chem. Chem. Phys.*, 1999, **1**, 3065.

Table 1: Calculated bond lengths (Å) and angles (º) of HBO-C, HBO-O and HBO-K

forms in the S_0 and S_1 states.

Electronic state	HBO-C		HBO-O		HBO-K	
	S_0	S_1	S_0	S_1	S_0	S_1
O-H	0.997	1.034	0.971	0.973	1.730	1.948
N⋯H	1.812	1.765	-	-	1.043	1.025
δ(O-H⋯N)	145.1º	147.4º	-	-	132.9º	125.2º

Table 2: The calculated primary bond lengths (Å) and angles (º) of BBHQ, BBHQ-A and BBHQ-B in the S_0 and S_1 states.

Electronic state	BBHQ		BBHQ-A		BBHQ-B	
	S_0	S_1	S_0	S_1	S_0	S_1
O_1-H_2	0.99	1.01	1.70	1.89	-	1.89
H_2-N_3	1.82	1.72	1.05	1.03	-	1.03
O_4-H_5	0.99	1.01	0.99	1.01	-	1.89
H_5-N_6	1.82	1.72	1.83	1.71	-	1.03
$\delta(O_1$-H_2-$N_3)$	144.8º	148.1º	134.1º	126.8º	-	127.1º
$\delta(O_4$-H_5-$N_6)$	144.8º	148.1º	145.2º	147.9º	-	127.1º

Table 3. Electronic excitation energy (nm), corresponding oscillator strengths and the corresponding compositions of the low-lying singlet excited states for BBHQ.

	Transition	λ(nm)	f	Composition	CI (%)
BBHQ	$S_0 \rightarrow S_1$	419	0.9597	$H \rightarrow L$	98.56%
	$S_0 \rightarrow S_2$	340	0.6945	$H\text{-}1 \rightarrow L$	97.44%
	$S_0 \rightarrow S_3$	302	0.0000	$H\text{-}2 \rightarrow L$	88.65%
				$H \rightarrow L+1$	10.13%

Figure captions

Figure 1. The optimized structures of HBO-C, HBO-O and HBO-K forms at the B3LYP/6-31+G(d)/IEF-PCM(heptane) theoretical level. Red: O; Gray: H; Blue: N; Black: C.

Figure 2. Variation of energy of HBO as a function of rotation of the torsional angle (θ) for transformation of the intramolecular hydrogen bonded HBO-C form to the non-hydrogen bonded HBO-O form as obtained at the B3LYP/6-31+G(d)/IEF-PCM(heptane) theoretical level.

Figure 3. (a) The calculated absorption and fluorescence spectra of HBO-C and HBO-K forms at the B3LYP/6-31+G(d)/IEF-PCM(heptane) theoretical level. The croci vertical lines show the experimental results. (b) The calculated frontier molecular orbitals HOMO and LUMO for HBO-C structure.

Figure 4. Potential energy curves of S_0 and S_1 states for HBO as a function of O-H bond length. The inset shows the corresponding potential barriers and the detailed potential energy curve of the S_1 state.

Figure 5. Optimized structures of BBHQ, BBHQ-A, BBHQ-B and the open form (BBHQ-Open) at the B3LYP/6-31+G(d)/IEF-PCM(heptane) theoretical level. Red: O; Gray: H; Blue: N; Black: C.

Figure 6. Calculated IR spectra of BBHQ in the spectral region of both O-H stretching bands in the S_0 and S_1 states based on the B3LYP/6-31+G(d)/IEF-PCM(heptane) theoretical level.

Figure 7. Frontier molecular orbitals, HOMO and LUMO, for the BBHQ chromophore based on TDDFT/B3LYP/6-31+G(d)/IEF-PCM(heptane) calculations.

Figure 8. PESs of the S_0 and S_1 states of BBHQ as functions of the O_1-H_2 and O_4-H_5 lengths from 0.79 to 2.09 Å. (a) S_1 state PES; (b) S_0 state PES. The red and yellow arrows indicates the direction of the S_1 state proton transfer.

Figure 9. The optimized structures of DHBO, DHBO-A (single proton transfer) and DHBO-B (double proton transfer) at the B3LYP/6-31+G(d)/IEF-PCM(heptane) theoretical level. Red: O; Gray: H; Blue: N; Black: C.

Figure 10. PESs of the S_0 and S_1 states of DHBO as functions of both O-H lengths ranging from 0.79 to 2.09 Å. (a) S_1 state PES; (b) S_0 state PES. The red and yellow arrows indicate the direction of the S_1 state proton transfer.
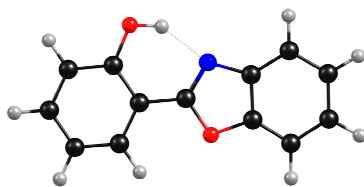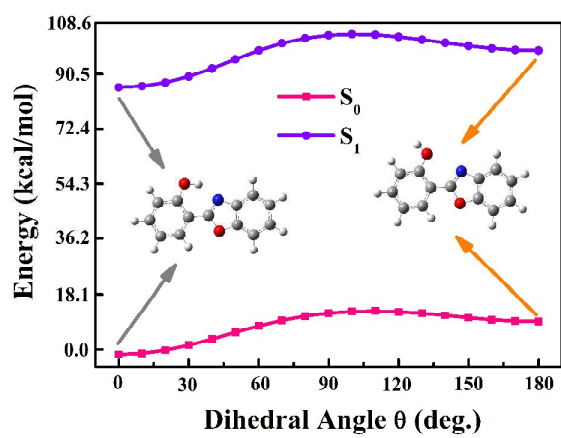
HBO-C
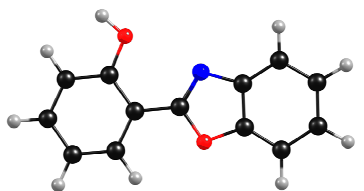
HBO-O
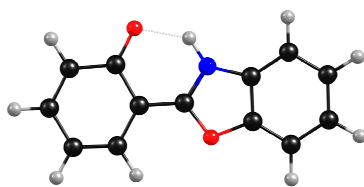
HBO-K

Figure 1

Figure 2

Figure 3

Figure 4

BBHQ

BBHQ−A

BBHQ−B

BBHQ−Open

Figure 5

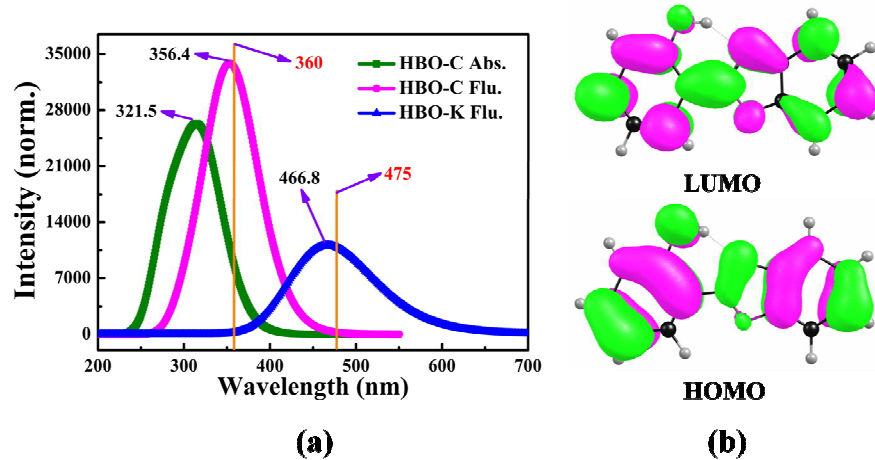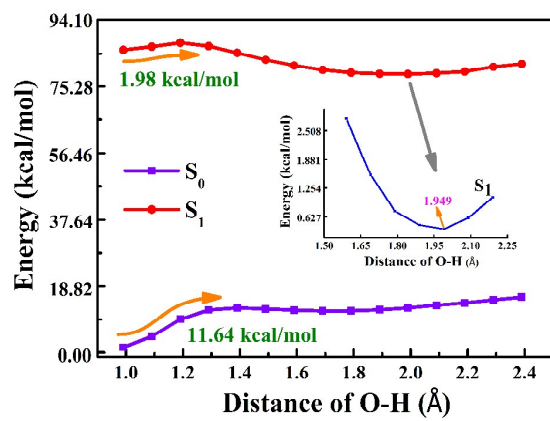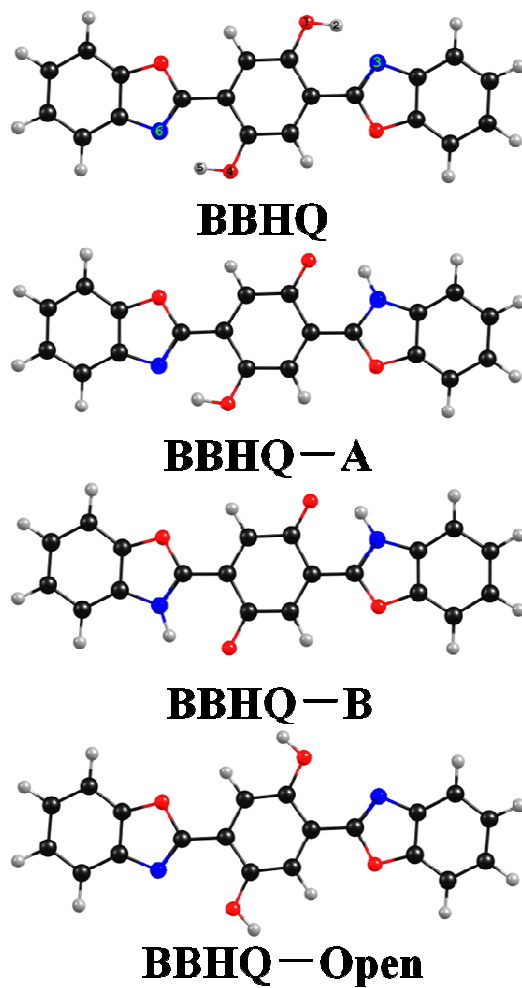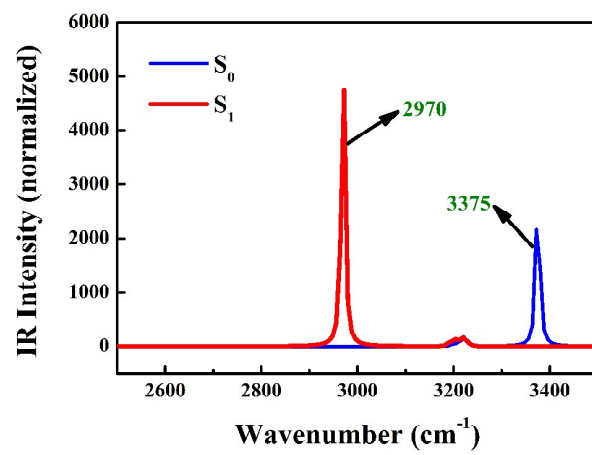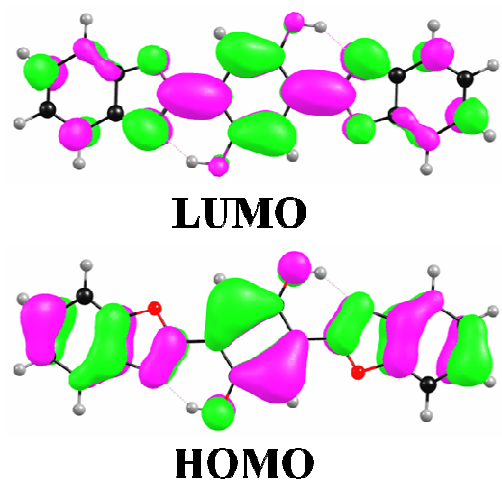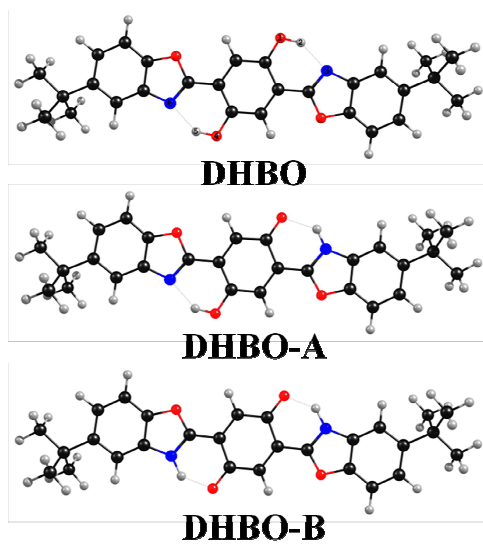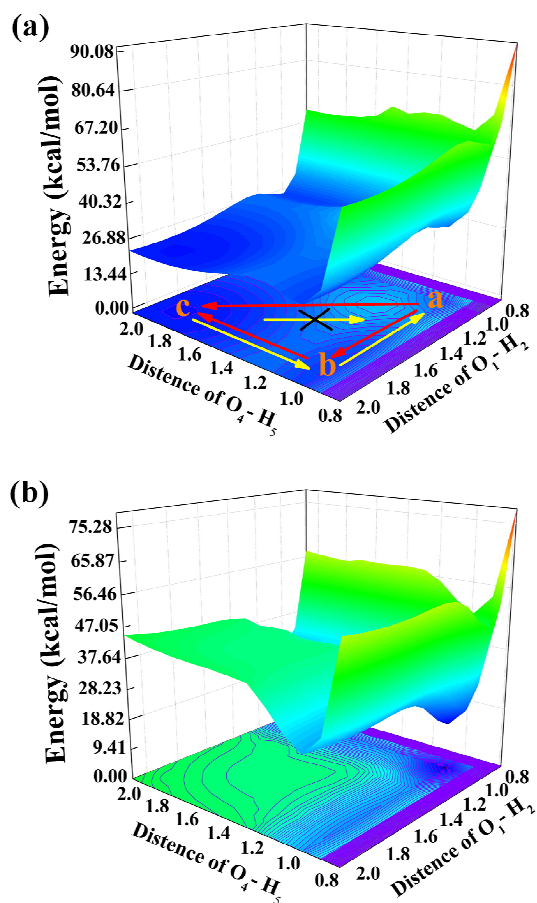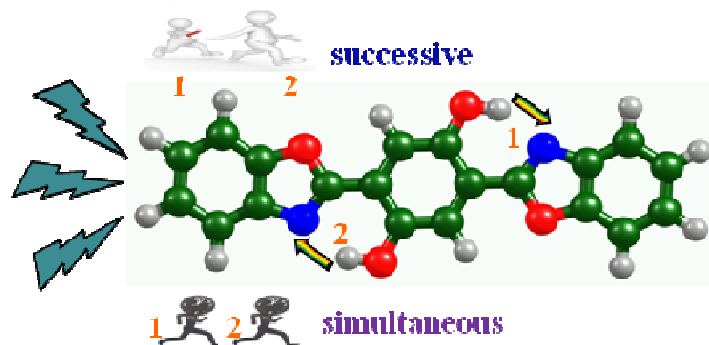Figure 6

Figure 7

Figure 8

Figure 9

(a)

(b)
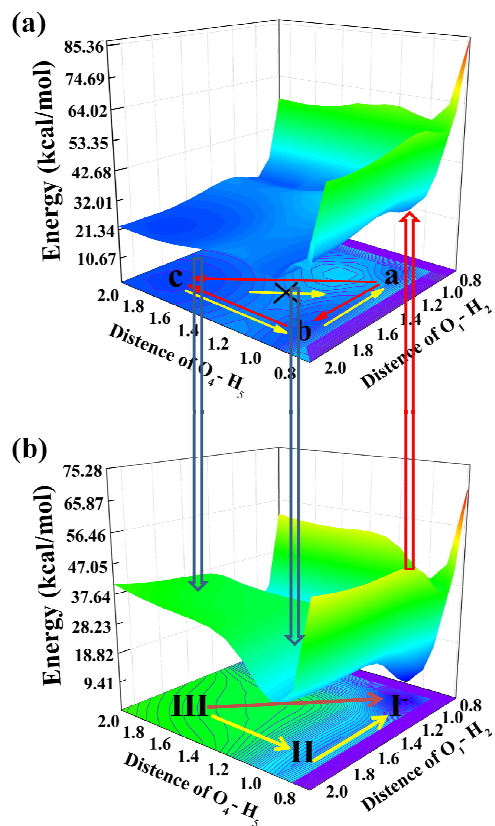
Figure 10

Schematic illustration